J Mater Sci (2006) 41:6385–6395
DOI 10.1007/s10853-006-0716-1

The aluminium effect on gel-derived iron silica glasses

M. G. Ferreira da Silva · M. A. Valente

Received: 20 May 2004 / Accepted: 13 July 2005 / Published online: 2 September 2006

Abstract Sol–gel aluminosilicate glasses containing 1 mol% of Fe_2O_3 and different amounts of Al_2O_3 (1; 2; 3; 4; 6 and 8 mol%) have been investigated. The ultraviolet–visible–near infrared spectrophotometry (UV–VIS–NIR), electron paramagnetic resonance (EPR), X-ray diffraction (XRD) and scanning electron microscopy (SEM), has been employed to obtain information about the structural evolution of the samples. The concentration of Al_2O_3, the treatment temperature and the furnace atmosphere play an important role in the structural incorporation of iron. The treatment of the samples, in air and under reducing conditions, results in remarkable changes in the UV–VIS–NIR and EPR spectra. In the samples were detected nanoparticles. The low temperature blocking of the nanoparticles magnetic moments has been clearly evidenced in the EPR derivative spectra at low temperatures.

Introduction

The study of iron containing silicate glasses, prepared by the sol–gel method, it is of great interest under the point of the view of its optical and magnetic properties [1–4]. We can obtain, by this method, glasses with finely dispersed magnetic nanoparticles. In iron containing aluminosilicate glasses the amount of Al^{3+} ions plays an important role in the formation of the magnetic nanoparticles because both, Fe^{3+} and Al^{3+} ions, can occupy tetrahedral and/or octahedral sites in the glass. If the amount of iron is maintained constant and the amount of aluminium changes what happens with the structural insertion of iron? Which is the structural evolution of the samples with the thermal treatment? The answer to these questions it is the main aim of the present investigation.

EPR spectroscopy is an effective technique to characterize the local structure of crystalline or vitreous materials [5–7]. The X-band EPR spectra of glasses with Fe^{3+} ions usually exhibit two well-defined lines at the effective g values $g_{eff} \approx 2.0$ and $g_{eff} \approx 4.3$ and a plateau extending to $g_{eff} \approx 10$ [6]. However, these EPR spectra, in different glasses matrix, show that the behaviour of this ion is quite different and complex. At low Fe^{3+} ion concentration, in borate glasses, only the $g_{eff} \approx 4.3$ line is observed [8–10]. On the other hand, in phosphate and silicate glasses the $g_{eff} \approx 2.0$ line is often present even at very low Fe_2O_3 contents [11–14].

The $g_{eff} \approx 4.3$ resonance has been assigned to tetracoordinated Fe^{3+} by various investigators [12] and to orthorhombic distortion of both tetrahedral and octahedral Fe^{3+} by others [15–18]. Similarly, the $g_{eff} \approx 2.0$ resonance has been interpreted as due to either octacoordinated Fe^{3+} [12, 15, 16], or ascribed to spin–spin interactions between Fe^{3+} ions as their average separation decreases [15, 17, 18]. Nevertheless, the EPR alone is clearly insufficient for a complete understanding of the behaviour of iron ions in the glass.

M. G. F. da Silva (✉)
Departamento de Engenharia Cerâmica e do Vidro, CICECO, Universidade de Aveiro, 3800-193 Aveiro, Portugal
e-mail: gsilva@cv.ua.pt

M. A. Valente
Departamento de Física, Universidade de Aveiro, 3800-193 Aveiro, Portugal

Thus, UV–VIS–NIR spectrophotometry is a complementary technique for the study of iron incorporation in transparent samples. SEM and XRD are also a good support in the characterization of the opaque samples.

In the present study, the structural evolution of SiO_2 gels containing 1 mol% Fe_2O_3 and different amounts of Al_2O_3, treated at different temperatures in air and reducing conditions, were studied by UV–VIS–NIR, XRD, SEM and EPR.

Experimental

Compositions indicated in Table 1. were prepared using as starting materials a solution of tetraethylorthosilicate (TEOS), ethanol (EtOH), water (H_2O), iron nitrate and aluminium nitrate. The molar ratio of TEOS:ETOH:H_2O was 1:3:4. The hydrolysis of TEOS is made in two steps. In the first step, a mixture of TEOS, EtOH and water in a molar ratio 1:3:1 was stirred for 1 h at room temperature. After this step the two nitrates, dissolved in water, were added to give a H_2O/TEOS ratio of 4. The solution was stirred for 1 h, poured into Petri dishes and allowed to gel and dried at 50 °C. The gel obtained was treated at 120 °C (48 h), between 250 °C and 800 °C (±5 °C) (4 h) and at 1000 °C (±5 °C) (2 h) under oxidizing (air-samples) and reducing conditions (red-samples) (10% H_2; 90% N_2).

The structure of the samples was examined using ultraviolet–visible–near infrared spectrophotometer (UV–VIS–NIR), electron paramagnetic resonance (EPR), X-ray diffraction (XRD) and scanning electron microscopy (SEM) techniques.

The UV–VIS–NIR measurements were carried out, at room temperature, using an UV–VIS–NIR UV-2101/3101PC spectrophotometer. XRD diffraction was performed at room temperature on a Rigaku XDMAX diffractometer using a monochromated CuKα radiation (λ = 1.5418 Å) at 40 kV and 30 mA, by step scanning (3 s–0.05°) using powdered samples. The SEM micrographs were obtained using an Hitachi S4100–1 electron microscope. The EPR measurements were carried out in a spectrometer (Brüker ESP 300E) operating at X band (9.7 GHz) with an Oxford Instruments variable temperature cryostat. The sample has been cooled down to a given temperature in zero magnetic field. The EPR spectra were acquired on finely powdered samples packed in quartz capillary tubes.

Table 1 Samples compositions (mol %)

Sample	Fe_2O_3	Al_2O_3	SiO_2
FA	1	1	98
F2A	1	2	97
F3A	1	3	96
F4A	1	4	95
F6A	1	6	93
F8A	1	8	91
2A	0	2	98
8A	0	8	92

Results

Colour of the samples

The colour of the samples, treated in air, is registered in the Table 2. The iron samples, treated in reducing conditions, have a dark-brown or black colour. Nevertheless, the F6A-250 °C and F8A–250 °C samples have, respectively, yellowish and orange colours.

Near infrared (NIR) spectrophotometry

The NIR spectra analysis permits to follow the gel-glass evolution. In all the 50 °C treated samples a band near 2300 nm (Fig. 1) is present. This band is due to the combination of stretching and deformation vibrations of the silanol groups (-Si-OH) bonded to water clusters [19]. This band was not observed for temperatures higher than 120 °C (Fig. 1). The 1900, 1460 and 1415 nm bands represent the combination of stretching and deformation vibration of silanol groups hydrogen bonded to water molecules [19]. These bands disappear at 800 °C (Fig. 1).

Free silanol groups are present in all the samples (bands around 2260, 2200 and 1380 nm [19]) (Fig. 1). However, in the 800 °C treated samples are only the bands around 2200 and 1380 nm (Fig. 1).

The bands, present in the 50 and 120 °C spectra, centred near 1756, 1726 and 1690 nm (Fig. 1), were associated to silanol groups linked to organic molecules [20].

Ultraviolet and visible spectrophotometry

A band near 450 nm was observed in all the 50 and 120 °C iron-containing samples (Figs. 2–5.). In the FA, F2A, F3A and F4A–250 °C spectra samples (Figs. 2 and 4), the absorption edge is shifted to longer wavelengths and the 450 nm band is not observed. This shift was not so evident in the F6A and F8A–250 °C spectra samples and the 450 nm band was observed (Fig. 5.). FA, F2A and F3A-500 °C spectra samples show a remarkable shift of the absorption edge to shorter wavelengths

Table 2 Colour of the transparent samples treated in air between 50 °C and 800 °C

Samples	Treatment temperature				
	50 °C	120 °C	250 °C	500 °C	800 °C
FA	Weak-tea	Amber	Brown	Yellowish	Ruby
F2A	Orange	Amber	Dark-brown	Yellowish	Dark-brown
F3A	Orange	Amber	Dark-brown	Yellowish	Brown-reddish[1]
F4A	Tea	Amber	Dark-brown	Yellowish	Brown
F6A	Weak-tea	Yellowish	Yellowish	Yellowish	Opaque (brown)
F8A	Orange	Yellowish	Orange	Orange	Brownish
2A	Colourless	Yellow	Brown	Tea	Opaque (white)
8A	Colourless	Colourless	Brown	Dark-brown	Dark-brown

[1] some pieces have a grey nucleus

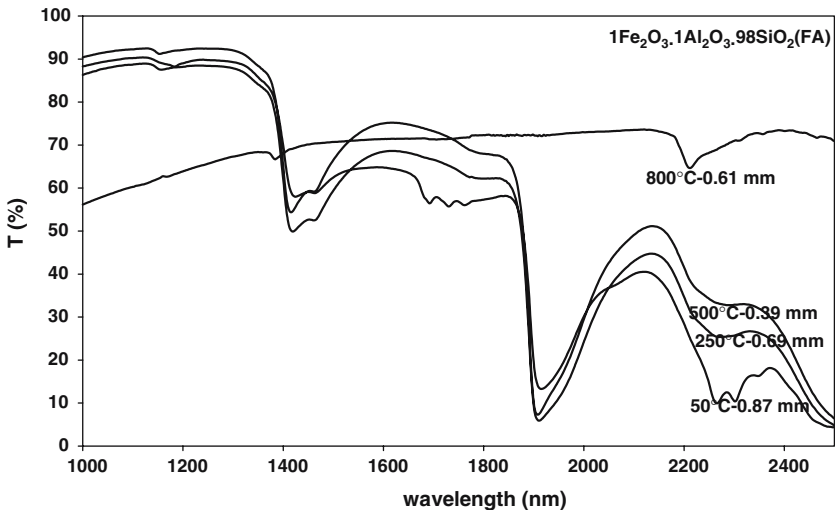

Fig. 1 NIR absorption spectra of the FA sample treated between 50 °C and 800 °C

(Figs. 2 and 3). In the samples treated at 500 °C, or at higher temperatures, the 450 nm band was not detected (Figs. 2–5.). One large band, near 880 nm, is present in the FA-800 °C spectrum (Fig. 6). In some spectra, including that of the 2A and 4A samples, appears a little band centred at 624 nm.

The spectra of the 2A and 8A samples (Figs. 7 and 8) exhibit a behaviour, with the treatment temperature, similar to that of the F2A and F8A samples, respectively. However, the 450 nm band is not present in these spectra.

In some spectra, including that of the 2A and 4A samples, appears a small band centred at 624 nm.

For the samples treated in reducing conditions it was only possible to register the 250 °C spectra, because the samples treated at higher temperatures are too darken colour.

XRD diffraction

All the iron containing samples, treated in air, maintain their transparency up to about 800 °C. However, the XRD patterns of the FA-1000 °C, F2A-1000 °C, F3A-1000 °C and F4A-1000 °C samples indicate the presence of α-cristobalite. When the amount of Al_2O_3 increases (case of the F6A-1000 °C and F8A-1000 °C samples) α-cristobalite and mullite are formed.

The crystalline phases that appear in the iron samples, treated at 1000 °C in reducing conditions, are the same formed in air. However, the F8A reducing sample shows a XRD pattern better defined than that of the F8A air sample.

Scanning electron microscopy

The samples treated in air have a very homogeneous structure up to 800 °C. However, at 1000 °C, it was possible to detect the presence of spherical particles and particles with a crystalline aspect. The micrograph of the FA-1000 °C sample (Fig. 9) shows the formation of particles with a crystalline aspect. In the F2A-1000 °C sample it was, also, possible to observe spherical particles (Fig. 10).

In the samples treated in reducing conditions the crystallization seems to begin at lower temperatures

than 1000 °C. Figure 11 shows the micrograph of the F2A-800 °C reducing sample.

Electron paramagnetic resonance

Samples treated in air

The EPR derivative spectra, at 300 K, of FA the samples treated between 50 °C and 1000 °C, are shown in Fig. 12. All the spectra have two resonances ($g_{eff} \approx 4.3$ and 2.0) and a shoulder ($g_{eff} \approx 10.0$), typical of Fe^{3+} ions in silicate glasses [6, 15, 16, 21]. The g factor, the linewidth (ΔH_{pp}) and the amplitude (A) of EPR signals, are calculated as described in a previous paper [21]. The ΔH_{pp} decreases from 250 to 39 gauss for the signal with $g_{eff} \approx 4.3$, and increases for the signal with $g_{eff} \approx 2.0$ with the increasing of the treatment temperature up to 800 °C. A narrowing of ΔH_{pp}, and a shift to lower resonance field ($g_{eff} \approx 2.11$), was observed in the sample treated at 1000 °C (Fig. 12). The EPR spectra of the F4A samples are similar to those of the FA samples (Fig. 12). However, a narrowing and a shift to lower fields, of the signal at $g_{eff} \approx 2.0$, was also observed in the samples treated at 800 °C. A weak hyperfine sextet at $g_{eff} \approx 2.0$, was detected in the FA, F2A, F3A, F4A samples treated at 250 and 500 °C (Figs. 12 and 13).

For the F2A-250 °C sample (Table 3) the ΔH_{pp} value of the $g_{eff} \approx 4.3$ signal is smaller than the ΔH_{pp} signal of the FA-250 °C sample. The behaviour of

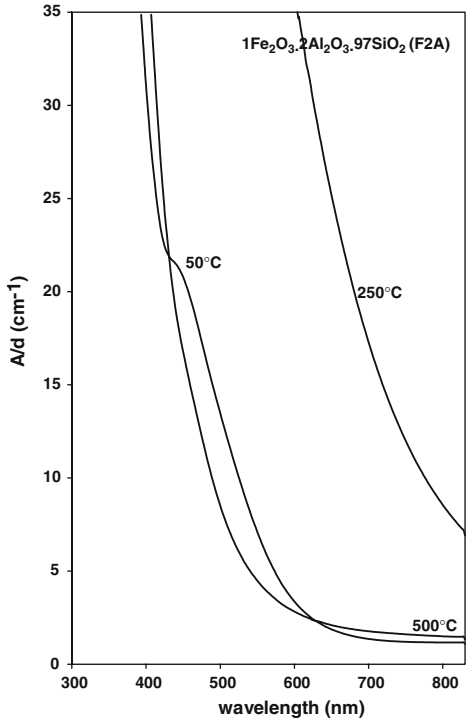

Fig. 3 UV–VIS absorption spectra of the F2A sample treated between 50 °C and 500 °C

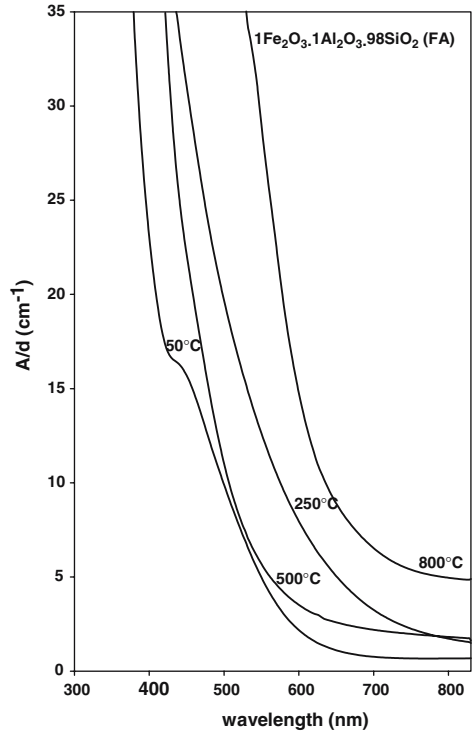

Fig. 2 UV–VIS absorption spectra of the FA sample treated between 50 °C and 800 °C

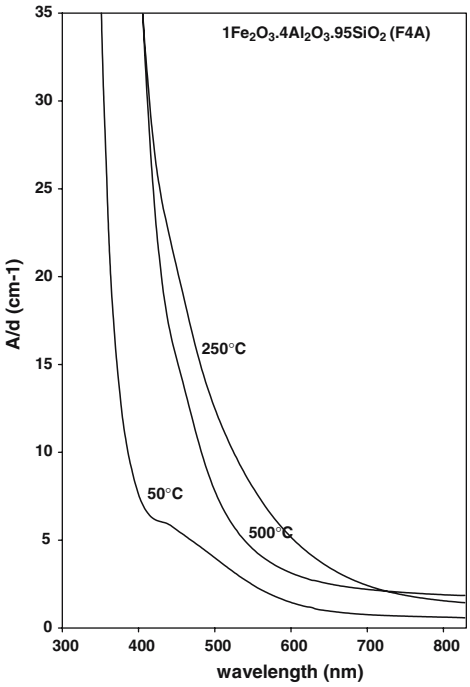

Fig. 4 UV–VIS absorption spectra of the F4A sample treated between 50 °C and 500 °C

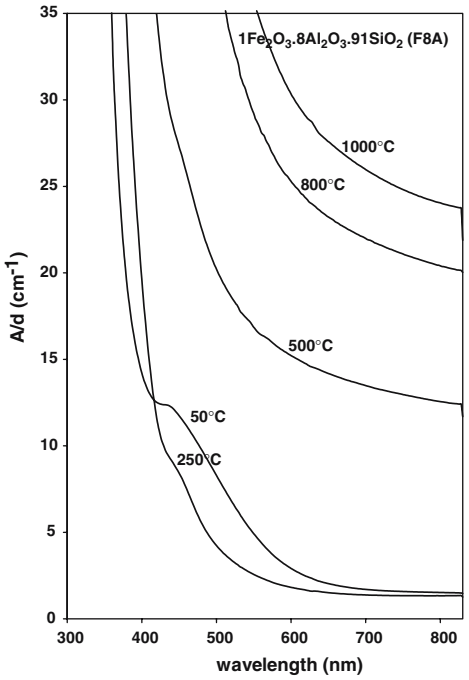

Fig. 5 UV–VIS absorption spectra of the FA sample treated between 50 °C and 1000 °C

ΔH_{pp}, of the signal with $g_{eff} \approx 4.3$, for the F2A and F3A samples is similar (Fig. 13). The F3A-800 °C sample has a $g_{eff} \approx 4.3$ signal with a very low amplitude and the signal with $g_{eff} \approx 2.0$ presents a very large amplitude (Fig. 13-right scale).

After a decreasing in the amplitude of the $g_{eff} \approx 4.3$ line, for the F6A-250 °C sample, it increases for the sample treated at 500 °C. The ΔH_{pp} decreases with the increasing of the treatment temperature. The sample treated at 500 °C has a narrow line with $g_{eff} \approx 2.0$ and the samples treated at 800 °C and 1000 °C present a broad signal with a very high amplitude. The sample treated at 1000°C shows also a shoulder at $g_{eff} \approx 3.13$.

For the F8A samples the amplitude of the signal at $g_{eff} \approx 4.30$ increases with the increasing of the treatment temperature, from 120 °C up to 500 °C, and ΔH_{pp} has an opposite behaviour. The signal centred at $g_{eff} \approx 2.0$ is broad with a small amplitude.

Figure 14 presents the spectra, at 300 K, of all the samples treated at 800 °C. The samples F3A and F6A have a weak signal at $g_{eff} \approx 4.3$ and a broad signal at $g_{eff} \approx 2.0$ with a very large intensity (Fig. 14-right scale).

In all the studied samples the signal at $g_{eff} \approx 4.3$ was improved when measurements were performed at temperatures below 300 K (Fig. 15). On the other hand, the behaviour of the $g_{eff} \approx 2.0$ signals is dependent of the composition of the sample and the treatment temperature. In the samples treated at 120 °C the amplitude of the EPR signal diminishes, under sample cooling, in the FA and F2A samples and increases in the F3A and F4A samples. This signal, in the F6A-120 °C sample, diminishes with the lowering of the temperature of measurement, from 300 K to 200 K, and then increases with the lowering of the measurement temperature. In the FA and F4A-800 °C samples the amplitude of the EPR signal increases under sample cooling and have a broadening and a shift towards high values, of the *g*-factor, in the F2A, F3A samples. In the F6A samples the signal increases with the lowering of the temperature of measurement, from 300 K to 200 K, and for them decreases with the reduction of the temperature of measurement. Figure 15 shows representative EPR derivative spectra of F3A-800°C samples obtained at different temperatures.

Samples treated under reducing conditions

A typical magnetic resonance spectra of the samples treated under reducing conditions is registered in

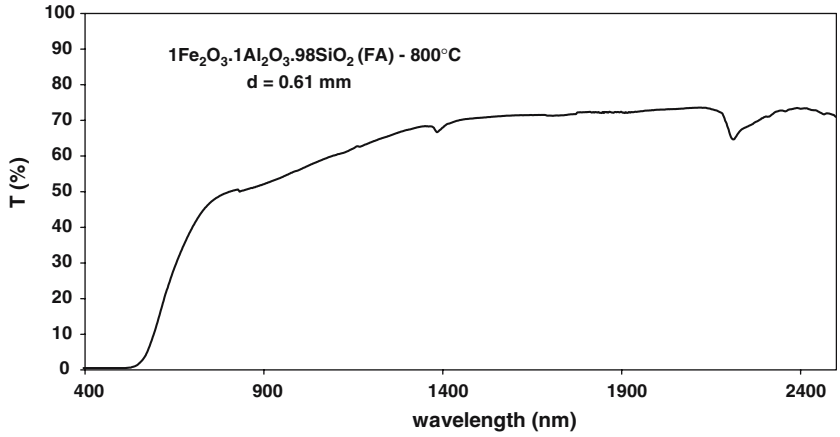

Fig. 6 UV–VIS–NIR absorption spectra of the F8A sample treated at 800 °C

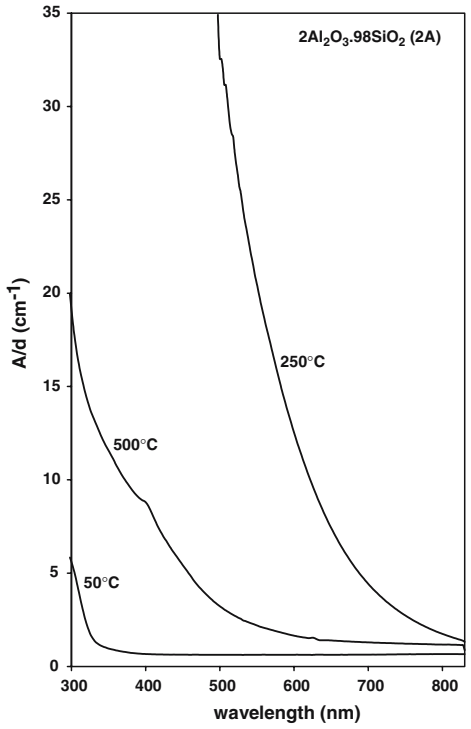

Fig. 7 UV–VIS absorption spectra of the FA sample treated between 50 °C and 500 °C

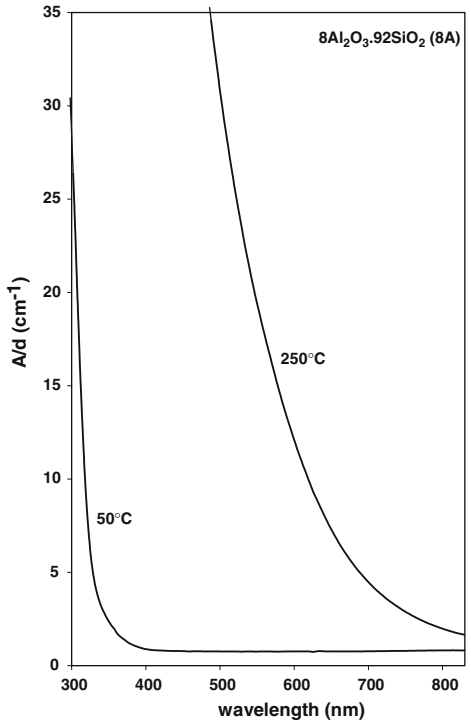

Fig. 8 UV–VIS absorption spectra of the FA sample treated at 50 and 250 °C

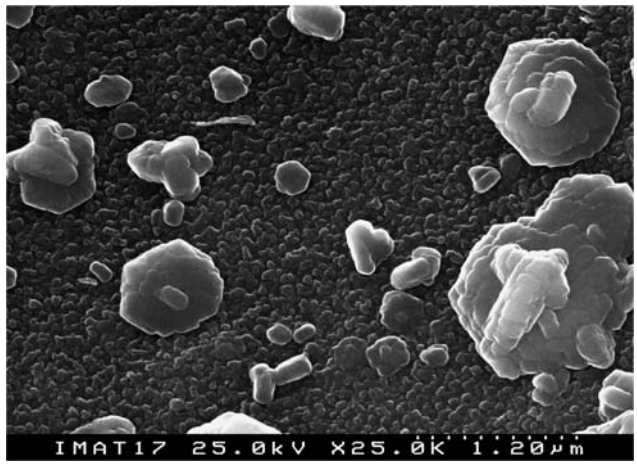

Fig. 9 SEM micrograph of the FA sample treated at 1000 °C

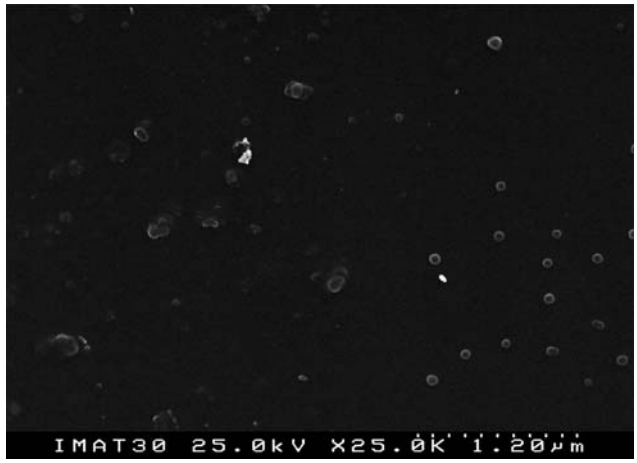

Fig. 10 SEM micrograph of the F2A sample treated at 1000 °C

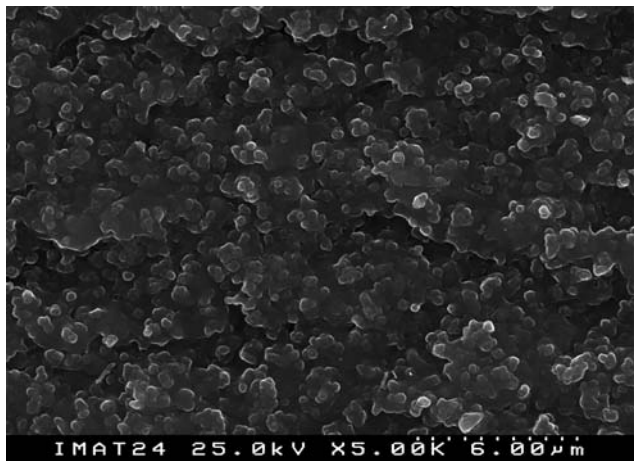

Fig. 11 SEM micrograph of the F2A sample treated at 800 °C in reducing conditions

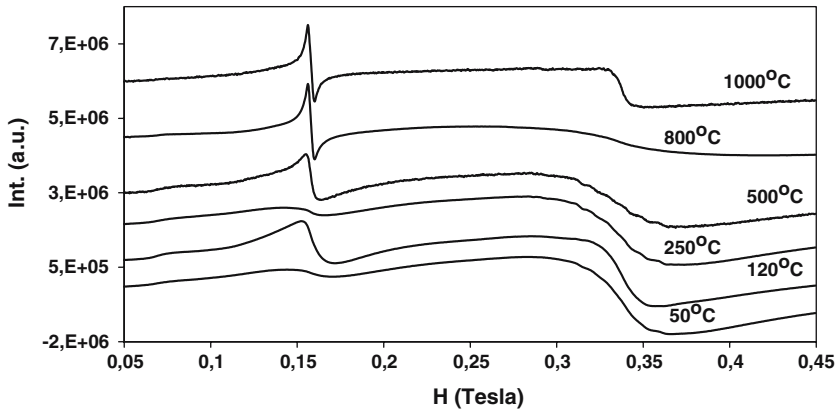

Fig. 12 Room temperature EPR derivate spectra, at room temperature, for the $1Fe_2O_3$ $1Al_2O_3$. $98SiO_2$ samples treated in air. Attenuation 10 dB; modulation frequency—100 kHz; modulation amplitude 10^{-3} Tesla and receiver gain 10^5

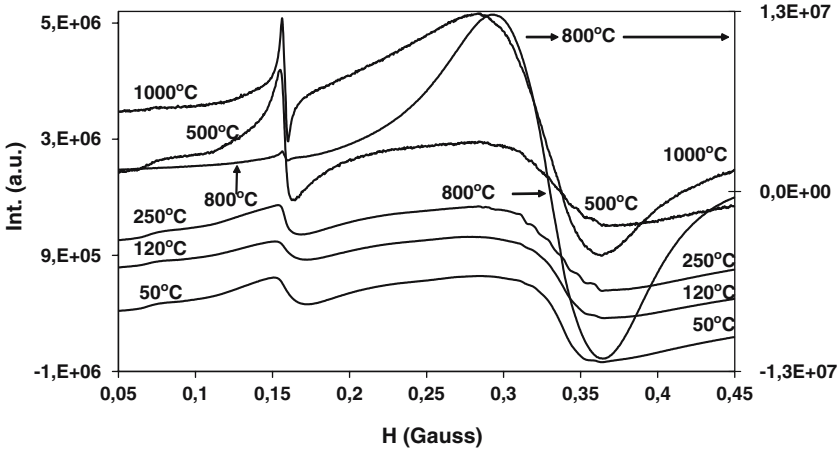

Fig. 13 Room temperature EPR derivate spectra, at room temperature, for the $1Fe_2O_3$ $3Al_2O_3$. $96SiO_2$ samples treated in air. Attenuation 10 dB; modulation frequency—100 kHz; modulation amplitude 10^{-3} Tesla and receiver gain 10^5

Table 3 The g values, the line width (ΔH_{pp}) and the EPR intensity (A) of the resonance absorption for the samples $1Fe_2O_3.2Al_2O_3$ 97 SiO_2 treated in air. Attenuation 10 dB; modulation frequency—100 kHz; modulation amplitude 10^{-3} Tesla and receiver gain 10^5 for all samples

Treatment temperature (°C)	$g \pm 0.02$	$(\Delta H_{pp}) \pm 4$ (10^{-4}Tesla)	I_{pp}*10^5He (a.u)	$A = I_{pp}x(\Delta H_{pp})^2$ (arbitrary units)
50	4.27	246	1.70	$10.3*10^9$
120	4.27	246	1.26	$7.63*10^9$
250	4.20	109	2.06	$2.45*10^9$
500	4.25	90	16.4	$1.32*10^9$
800	4.27	39	26.1	$3.99*10^9$
1000	4.27	39	20.2	$3.09*10^9$
50	2.09	801	16	$10.3*10^{11}$
120	1.99	528	8.9	$2.5*10^{11}$
250	2.07	754	12.1	$6.88*10^{11}$
500	2.09	805	17.8	$11.5*10^{11}$
800	1.99	1150	8.9	$11.9*10^{11}$
1000	1.98	183	11.4	$0.382*10^{11}$

Fig. 16 (F2A). The spectra of the samples treated up to 500 °C have two resonances ($g_{eff} \approx 4.3$ and $g_{eff} \approx 2.0$) and a weak hyperfine sextet at $g_{eff} \approx 2.0$ (Fig. 16). The samples treated at 500 °C show at $g_{eff} \approx 2.0$ a narrow and well resolved line, superimposed on a broad line, and the samples treated at 800 °C show a narrow and well resolved line. For the samples (FA, F3A, F4A, F6A) treated at 1000 °C the line at $g_{eff} \approx 2.0$ has a small value or is about zero (F2A and F8A samples).

The signal with $g_{eff} \approx 2.0$ is not significantly affected by the lowering of the temperature of measurement. A tenuous signal at $g_{eff} \approx 4.30$ increases with the lowering of the temperature of measurements.

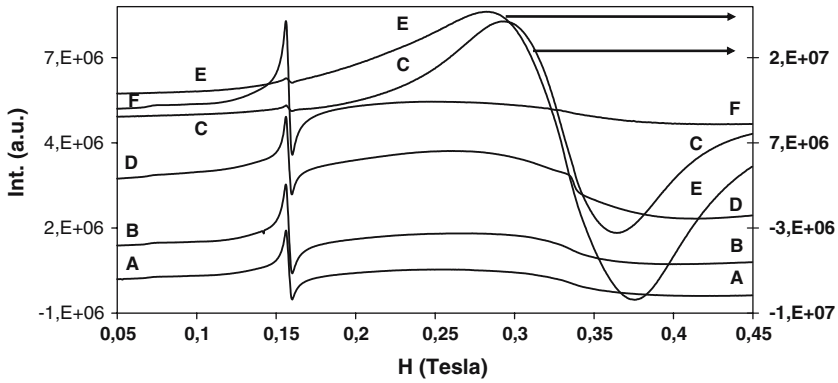

Fig. 14 Room temperature EPR derivate spectra, at room temperature, for all samples treated in air at 800 °C. Attenuation 10 dB; modulation frequency—100 kHz; modulation amplitude 10^{-3} Tesla and receiver gain 10^5

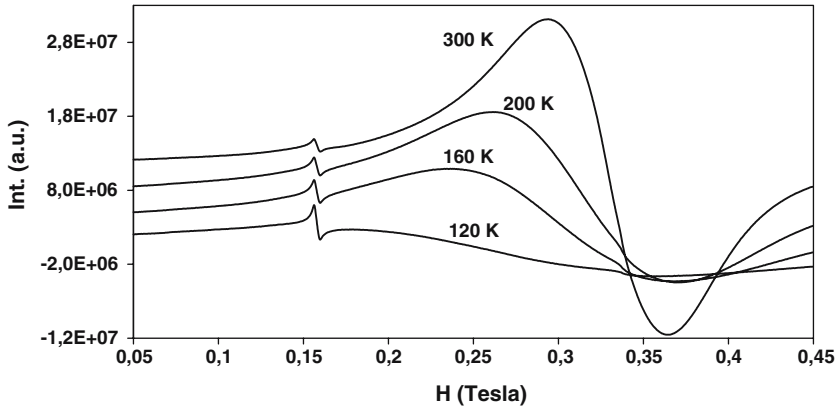

Fig. 15 EPR derivate spectra, for sample F3A treated in air at 800°C at different temperatures indicated in the right side of the curves. Attenuation 10 dB; modulation frequency—100 kHz; modulation amplitude 10^{-3} Tesla and receiver gain 10^5

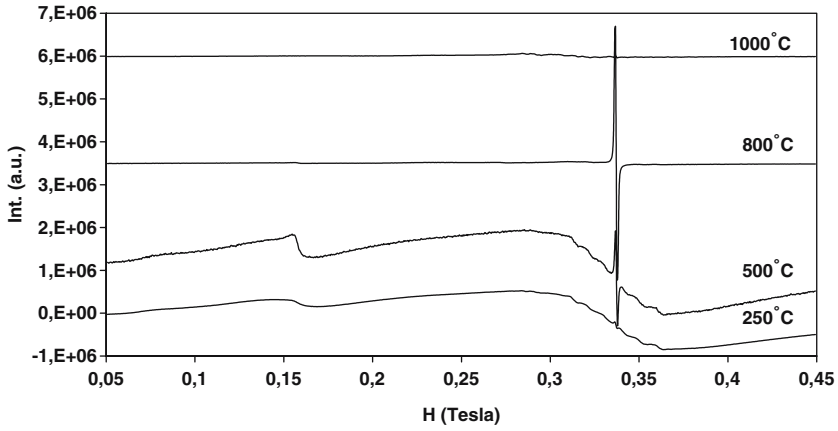

Fig. 16 EPR derivate spectra, at room temperature, for the $1Fe_2O_3$ $2Al_2O_3$. $97SiO_2$ samples treated in reduction condition. Attenuation 10 dB; modulation frequency—100 kHz; modulation amplitude 10^{-3} Tesla and receiver gain 10^5

Discussion

The iron containing samples treated in air, at 50 and 120 °C, show an absorption band near 450 nm (VIS spectra—Figs. 2–6) and two EPR signals with $g_{eff} \approx 2.0$ and 4.3. The band centred at 450 nm (Fig. 5) belongs to the Fe^{3+} ion in tetrahedral coordination ($^6A_1$ - > ^4E, $^4A_1$) and was observed in silicate glasses [22]. The absorption band near 450 nm, and the EPR signal at 4.3, can be connected to the occurrence of Fe^{3+} as $[Fe(OH)_4]^-$ tetrahedral complexes. The $g_{eff} \approx 2.0$ strong and broad signal is associated to the presence of agglomerates of iron small particles as already observed in materials with a similar composition [23]. However, this signal can be also associated to the presence of the iron ions as $[Fe(H_2O)_x(OH)_{6-x}]^{3+}$ and $[Fe(H_2O)_6]^{3+}$ octahedral complexes. The VIS bands of Fe^{3+} in octahedral coordination are not detected in the spectra because the band centred at 450 nm could mask the bands due to Fe^{3+} in octahedral coordination. The presence of $[Fe(H_2O)_x(OH)_{6-x}]^{3+}$ and $[Fe(H_2O)_6]^{3+}$ octahedral complexes and $[Fe(OH)_4]^-$

tetrahedral complexes, in the referred samples, it is justified by the fact that in the NIR spectra it is evident the existence of a great amount of water and silanol groups (bands at 2300, 1900, 1460 and 1415 nm—Fig. 1). The FA-120 °C, F2A-120 °C, F3A-120 °C and F4A-120 °C samples acquire an amber colour. The 2A-120 °C, F6A-120 °C and F8A-120 °C samples are yellow and the 8A-120 °C sample is colourless. How to explain this diversity of colours? The answer can be: the samples colour is attributed, simultaneously, to the presence of the nitrogen oxides (NO_2 and N_2O_4), iron agglomerates and Fe^{3+} complexes. Analysing the colour and the VIS spectra of the 2A samples (Fig. 4) we can say that, with the increasing of the treatment temperature, up to 250 °C, the amount of NO_2 increases, the sample becomes darker and the absorption edge suffers a notorious shift to 600 nm due to the presence of NO_2 (brown gas) as result of the nitrate decomposition [24]. On the other hand the 8A sample is colourless at 120 °C and brown at 250 °C (Table 2) because the large nitrate content of this sample induces the formation of N_2O_4 (colourless gas) at 120 °C. At 250 °C, probably, some nitrogen oxide escapes outward the sample and the amount of NO_2 increases. The presence of NO_2 molecules is also confirmed by the weak sextet observed in the EPR spectra of the F2A-250 °C, F3A-250 °C and F4A-250 °C (Fig. 13) [25–28]. The difference in the behaviour of the nitrogen oxides in the studied samples can be related with the structure of the samples. ^{27}Al nuclear magnetic resonance studies of binary Al_2O_3–SiO_2 samples [29] prove that the rate between the aluminium in tetrahedral sites and that in octahedral sites depends on the amount of Al_2O_3 and the treatment temperature of the sample. Iron affects also the structural evolution of the samples because the 8A and the F8A-250 °C samples have not the expected colours. The 8A-250 °C sample has a brown colour and the F8A-250 °C is orange. This means that, in the 8A sample, is present a great amount of NO_2 than in the F8A sample. F6A and F8A samples, treated at 120 and 250 °C, are yellowish and orange, probably, by the same reason as F4A-250 °C sample is dark brown. Thus, the large nitrate content of the F6A and F8A samples make possible only the formation of N_2O_4 (colourless gas) or, due to the structure of the samples, nitrogen oxides escape outward the samples. In the F6A-250 °C and F8A-250 °C VIS spectra (Fig. 4) it was not observed a considerable dislocation of the VIS absorption edge, between 50 °C and 250 °C, because the brown gas (NO_2) is not, apparently, present and the colour of the samples is only due to the presence of iron oxide agglomerates and Fe^{3+} complexes. At 500 °C, when the samples porosity, probably, reaches a maximum [30], the nitrogen oxides escape out of the samples FA, F2A, F3A, F4A and 2A, but remain into the dark-brown 8A sample. At 800 °C, the samples suffer a strong shrinkage and, a lot of NO_2 can remain into the structure. When the treatment temperature of the samples increases, the amplitude of the $g \approx 4.3$ EPR signal increases up to 500 °C. This increasing is related with the dissolution of iron agglomerate particles [23] and the concomitant increasing of the tetrahedral coordinated Fe^{3+}. In the samples FA, F2A, F3A and F4A, treated up to 500 °C, the EPR line at $g_{eff} \approx 2.0$ is a superposition of two spectra, a broad one due to iron oxide agglomerates and Fe^{3+} and a weak sextet attributed to the presence of NO_2 molecules [25–28]. Around 800 °C the porous network densifie, the water and the OH groups are almost eliminated (Fig. 9), and this fact has a strong influence in the structure of the samples. The FA-800 °C sample has a ruby colour as that observed in similar composition samples without aluminium [23] and the VIS spectra show a notorious shift of the absorption edge, between 500 °C and 800 °C, and a large band centred at 880 nm associated to the presence of colloidal particles [23]. The brown colour and the broad signal with $g_{eff} \approx 2.0$, of the F2A-800 °C, F3A-800 °C, F4A-800 °C, F6A-800 °C and F8A-800 °C samples, suggest the presence of greater particles in these samples than in FA-800 °C sample. This behaviour can be explained having in account that the F6A and F8A samples have more aluminium than the others samples. Thus, because the aluminium ions occupy, simultaneously, octahedral and tetrahedral sites in the silicate network and the Fe^{3+} ions are, normally, incorporated into the silica-glass network in tetrahedral coordination [23] the presence of more Al^{3+} in tetrahedral sites can make difficult the incorporation of iron ions and to promote the iron oxide segregation. Therefore, the iron incorporation is, at 800 °C, strongly dependent on the amount of aluminium present in the samples. Also the observed decreasing, in the linewidth of $g_{eff} \approx 4.3$ signal, with the increasing of the treatment temperature can be attributed to the decreasing of the Fe^{3+} ions incorporated in the vitreous network [17, 31]. The F3A and F6A samples seem to have a stronger tendency to be opaque than the other iron samples, because F6A-800 °C is the only opaque and some pieces of F3A-800 °C have a grey nucleus. Also, for these two samples the $g_{eff} \approx 2.0$ EPR signal is broad and very strong. For the F2A-800 °C, F3A-800 °C and F6A-800 °C samples the $g_{eff} \approx 2.0$ signal present a decreasing of the amplitude and a broadening, under sample cooling (Fig. 15). The narrow and broad $g_{eff} \approx 2.0$ signal resonance is the signature of

paramagnetic or superparamagnetic particles imbedded in a more or less crystallized matrix [32–34]. The decreasing in the amplitude of the $g_{eff} \approx 2.0$ signal takes place at the same time as the ΔH_{pp} increases and the signals suffer a shift to lower fields (fig.15). The behaviour of the EPR line at $g_{eff} \approx 2.0$, with the temperature, proves the presence of superparamagnetic particles in the samples [35, 36]. The lack of a narrow resonance could be due to the size of the particles [35, 36]. The superparamagnetic behaviour is observed for the particles with diameters less than ≈15 nm. The magnetic moment of such a particle is subject to thermal fluctuations resulting in motional narrowing of the EPR spectra. From a magnetic point of view and according to Néel's theory, small-size particles are single domain at low temperatures [37]. The appearance of an EPR signal with $g \approx 3.13$ for the F6A-1000 °C sample is in good agreement with the theoretical possibility of obtaining isotropic g-values of 2, 10/3 and 30/7, for $3d^5$ ions [15]. The resonance at $g \approx 10/3$ can be ascribed to tetragonal, trigonal or ortorombic sites properties [15].

For the samples treated in reducing conditions the narrow EPR line can be due to superparamagnetic nanoparticles [30]. This line can be attributed to the presence, in the glass, of Fe_3O_4 or/and Fe particles, which behaves as superparamagnetic particles. The broad signal, at $g_{eff} \approx 2.0$, observed in the samples treated in reducing conditions, below 500 °C, can be associated to the presence of iron agglomerates as in the case of the air samples treated to the same temperature.

The behaviour of the EPR signal at $g_{eff} \approx 2.0$, with the temperature of measurement, for all the samples, can be attributed to the presence of a wide range of iron particle sizes. Thus, changes of particles size, or changes of temperature, promote changes in the EPR spectra (paramagnetic state is replaced by the superparamagnetic state).

The glass matrix of the samples suffers crystallization at 1000 °C. Thus, the XRD patterns show the presence of cristobalite and mullite and in the micrographs were detected particles with a crystalline aspect (Fig. 9). Also, spherical particles were observed, by SEM, in the samples (Fig. 10). This spherical particles were related with the presence of iron oxide particles in the samples.

Conclusions

The colour diversity of the samples can be attributed, simultaneously, to the presence of the nitrogen oxides (NO_2 and N_2O_4), iron agglomerates and Fe^{3+} ions complexes. In the samples treated in air, at 50 and 120 °C, the iron can be present as iron agglomerates, $[Fe(H_2O)_x(OH)_{6-x}]^{3+}$ and $[Fe(H_2O)_6]^{3+}$ octahedral complexes or $Fe(OH)_4]^-$ tetrahedral complexes. When the samples treatment temperature increases, from 50 °C to 500 °C, the amount of $[Fe(OH)_4]^-$ complexes increases. Around 800 °C the porous network densifie and iron oxide particles are segregated. Also, the presence of aluminium can make difficult the incorporation of iron ions and to promote the iron oxide segregation.

In all the samples (treated in air or under reducing conditions) it was detected the presence of superparamagnetic particles.

References

1. Encheva G, Samuneva B, Djambaski P, Kashchieva E, Paneva D, Mitov I (2004) J Non-Cryst Sol 345:615
2. Sanchez SAP, Castañeda SP, Martınez JR, Ruiz F, Chumakov Y, Domınguez O (2003) J Non-Cryst Sol 325:251
3. Lutz T, Estournés C, Guille JL (1998) J Sol–Gel Sci Technol 13:929
4. Niznansky D, Viart N, Rehspriger JL (1997) J Sol–Gel Sci Technol 8:615
5. Bolton JR, Wertz JE (1994) Electron paramagnetic resonance, elementary theory and practical applications. John Willey, New York
6. Griscom DL (1980) J Non-Cryst Sol 40:211
7. Griscom DL (1985) J Non-Cryst Sol 73:51
8. Rao JL, Murali A, Rao ED (1996) J Non-Cryst Sol 202:215
9. Peteanu M, Cociu L, Ardelean I (1994) J Mater Sci Technol 10: 97
10. Berger R, Kliava J, Yahiaoui EM, Bissey JC, Zinsou PK, Béziade P (1995) J Non-Cryst Sol 180:151
11. Kliava J, Berger R, Servant Y, Emery J, Grenèche JM Trokss J (1996) J Non-Cryst Sol 202:205
12. Camara B, Oel HJ (1984) J Non-Cryst Sol 65:161
13. Tanabe S, Hirao K, Soga N (1988) J Non-Cryst Sol 100:388
14. Tanaka K, Kamiya K, Matsuoka M, Yoko T (1987) J Non-Cryst Sol 94:365
15. Roy S, Ganguli D (1996) J Non-Cryst Sol 195:38
16. Montenero A, Friggeri M, Giori DC, Belkhiria N, Pye LD (1986) J Non-Cryst Sol 84:45
17. Mendiratta SK, Sousa EG (1988) J Mater Sci Lett 7:733
18. Tanaka K, Kamiya K, Yoko T, Tanabe S, Hirao K, Soga N (1991) Phys Chem Glass 32(1):16
19. Wood DL, Rabinovich EM, Johnson DW JR., Machesney JB, Vogel EM (1983) J Am Ceram Soc 66:693
20. Ferreira da Silva MG (2001) J Mater Sci 36:3247
21. Ferreira da Silva MG, Valente MA (2000) J of Sol-Gel Sci Technol 17:47
22. Barbieri L, Bianchi CL, Bruni S, Cariati F, Leonelli C, Manfredini T, Paganelli M, Pellacani GP, Russo U (1993) J Non-Cryst Sol 155:231
23. Ferreira da Silva MG, Navarro JMF (1996) J Sol-Gel Sci and Technol 6:169
24. Cotton FA, Wilkinson G (1972) Advanced inorganic chemistry. Interscience Publishers, New York
25. Griscom DL (1978) J Non-Cryst Sol 31:241

26. Friebele EJ, Griscon DL, Hickmott TW (1985) J Non- Cryst Sol 71:351
27. Hosono H, Abe Y (1991) Phys Rev B 43(14):11966
28. Bogomolova L, Jachkin VA, Prushinsky SA, Stefanovsky SV, Teplyakov YG, Teplyakov YG, Caccavale F (1997) J Non- Cryst Sol 220:109
29. M.G. Ferreira da Silva - to be published
30. Klein LC, Gallo TA, Garvey GJ (1964) J Non-Cryst Sol 63:23
31. Parekh K, Upadhyay RV, Mehta RV, Srinivas D (2000) J Appl Phys 88 (5):2799
32. Berger R, Bissey JC, Kliava J, Soulard B (2001) J Magm Magn Mater 167:129
33. Berger R, Kliava J, Bissey JC, Baïetto V (1998) J Phys Condens Matter 10:8559
34. Berger R, Kliava J, Bissey JC, Baïetto V (2000) J Appl Phys 87(10):7389
35. Koksharov YA, Gubin SP, Kosobudsky ID, Beltran M, Khodorkovsky Y, Tishin AM (2000) J Appl Phys 88 3, 1:1587
36. Berger R, Bissey JC, Kliava J, Daubric H, Estournès C (2001) J Magm Magn Mater 234:535
37. Bentivegna F, Ferré J, Nývlt M, Jamet JP, Imhoff D, Canva M, Brun A, Veillet P, Visnovsky S, Chaput F, Boilot JP (1998) J Appl Phys 7776: 83–12